Materials Research Express

PAPER

Millepore species-like ultra-long carbon fiber/cobalt nickel and its electrochemical activity

To cite this article: Chi Yang *et al* 2019 *Mater. Res. Express* **6** 115621

Materials Research Express

RECEIVED
4 June 2019

REVISED
18 October 2019

ACCEPTED FOR PUBLICATION
23 October 2019

PUBLISHED
1 November 2019

PAPER

Millepore species-like ultra-long carbon fiber/cobalt nickel and its electrochemical activity

Chi Yang[1], **XiaoHong Sun**[1,2] **and ChunYan Zhang**[1]

[1] Yale-NUIST Center on Atmospheric Environment, International Joint Laboratory on Climate and Environment Change (ILCEC), Nanjing University of Information Science and Technology, Nanjing 210044, People's Republic of China
[2] School of Pharmacy, Anhui University of Traditional Chinese Medicine, Hefei 230031, People's Republic of China

E-mail: yangchi@seu.edu.cn

Keywords: ultra-long, NiCo precursor, DA, UA, millepore sp. -like

Abstract

An ultra-long NiCo precursor having a morphology similar to *Millepore species (Millipore sp.)* was prepared to utilize a green homogeneous precipitation method. The *Millepore species* -like component is $[MCO_3]x \cdot [M(OH)_2]y \cdot nH_2O$ (M = Co, Ni; x, y, n = 1–5), which is a precursor of NiCo metal compounds, hydroxides, and oxides. There is no organic residue in the prepared product, making this synthetic procedure green. At the same time, the precursor grown *in situ* on carbon fiber produces ordered and controllable *Millepore sp.*-like materials as well as a stand-by electrode. The resistance of the adhesive bond to the glassy carbon electrode by the cobalt-nickel material is avoided. Following electrochemical activity tests, the *Millepore sp.*-like NiCo precursor showed significant redox activity on dopamine and uric acid. Differential pulse voltammetry can simultaneously detect two substances with excellent linear at the range of uric acid 0.04–0.2 mM and dopamine 6–20 μM.

1. Introduction

The preparation of ultra-long structural materials is conducive to expanding its application in the macroscopic field of electronic processing and biosensors and can be better combined with general technology [1]. At the same time, most modified electrodes combine the modified material with an electrode such as glassy carbon using an adhesive. The addition of the adhesive reduces the electron transport process between the modified material and the electrode, which increases the electron retarding effect of the modified electrode [2]. Therefore, an ultra-long structure grown *in situ* can prevent low electrochemical activity caused by the binder [3], while the 3D nanostructure grown on the surface helps prevent the electrode from collapsing and enhances the electrochemical activity [4]. For example, Fan *et al* [5] prepared a gas sensor based on ultra-long Zn_2SnO_4-ZnO, which has high sensitivity and selectivity to hydrogen. Yang *et al* [6] achieved a low detection limit for trimethylamine using an ultra-long MoO_3 material. Wang *et al* [7] observed high sensitivity to gas and light through the preparation of ultra-long, single-crystal Ag_2S nanowires. So far, there have been few NiCo composites for ultra-long porous structures.

Co and Ni have attracted extensive attention due to their unique atomic arrangement and productive valence state transformations in materials such as alloys [8], hydroxides [9], and oxides [10]. The hollow structures [11, 12], hierarchical structures [13–15], and core–shell structures [16, 17] of these materials have been reported in the energy storage and conversion devices [18–21] and electrochemical sensing [22–24] fields. For example, A lower detection limit (0.42 nM) for estriol in milk was established using NiCo oxide nanoflakes prepared by Fu *et al* [25]. The excellent electrochemical activity of NiCo materials is due to the synergistic redox reaction between them; this reduces the energy barrier of single Co/Ni materials with a substrate [26]. In addition to the synergistic effect of bimetals, morphology, and structure play an essential role in the electrochemical activity of NiCo materials. Joseph *et al* [27] prepared a NiCo hydroxide with a porous structure, a capacitance of 1380 Fg^{-1}, and achieved 5,000 stable cycles in the electrolyte. However, the NiCo hydroxide/carbon with an ultra-lamellar structure achieved a sphere capacitance of only 957 Fg^{-1} and stable for 3000 cycles

[28]. In short, the higher comparison area, thus reducing the ion diffusion distance, has led to widespread interest in modifying electrode materials.

The NiCo mentioned above was obtained by chemical reaction of Ni/Co salts; then, applying different morphologies of material formation were studied. Most materials were obtained hydrothermally followed by precipitation; the hydroxide is then obtained by loss of carbonate at lower temperatures while the oxide is obtained by further heating at higher temperatures. However, none of these efforts pay attention to the performance of the precursor. Here, we prepared this precursor material, especially the carbon fiber as a template to prepare an ultra-long, ordered cobalt-nickel/carbon precursor fiber (NiCo precursor/C). We expect that the NiCo on the microscopic surface is porous, and the carbon fiber integrates into the material in an orderly manner producing an ultra-long structure as a stand-by electrode. Finally, the electrochemical activity of this composite was verified by electrochemical detection of dopamine (DA) and uric acid (UA).

2. Experimental process

2.1. Reagents and apparatus

All chemical reagents used were analytical grade and used without further purification; high purity water (MiliQ system, Millipore Co.) was used throughout. Nickel nitrate ($Ni(NO_3)_2{\cdot}6H_2O$), cobalt nitrate ($Co(NO_3)_2{\cdot}6H_2O$) (Zhongguo Group Chemical Fiber Reagent Co., Ltd) and urea (Zhongguo Group Chemical Fiber Reagent Co., Ltd) was used as synthetic precursors. NiCo was generated *in situ* on purchased carbon fibers (Jiangsu Sutong Carbon Fiber Co., Ltd).

X-ray photoelectron spectroscopy (XPS, Thermo ESCALAB 250), x-ray diffractometry (XRD, Rigaku D max/RB, Cu palladium Kα ray, $\lambda = 0.1542$ nm, V = 36 kV, I = 30 mA) and FTIR (Nicolet FTIR-NEXU 670, 4000–400 cm^{-1}, room temperature) were used to characterize prepared samples. Field emission scanning electron microscopy (FE-SEM, Hitachi S-4800, 5 kV) was used to study sample morphology.

2.2. *In situ* synthesis of the NiCo precursor/C working electrodes

A carbon fiber (~0.1 g) and approximately 5 cm long, 4–5 μm in diameter (depending on growth time) was added to a solution with 0.01 mol l^{-1} nickel nitrate, 0.02 mol l^{-1} cobalt nitrate, and 1.2 mol l^{-1} urea; this solution was ultrasonically dispersed for 1 h. The reaction temperature was controlled at 90 °C and magnetically stirred; precipitation was ended once the upper layer was colorless. After filtering the product, it was washed several times with ethanol and deionized water, respectively. Then placed in an oven and dried at 60 °C for 10 h to obtain the target product. The obtained NiCo precursor/C can be directly used as a working electrode without any further treatment, and the electrode is represented by a NiCo precursor/C (figure 1). When not in use, the electrode was placed in a 0.1 M phosphate buffer and stored at 4 °C.

2.3. Electrochemical experiments

The electrochemical properties of prepared materials were measured using a CHI-660E electrochemical workstation (Shanghai Chenhua); those properties included cyclic voltammetry (CV) and differential pulse voltammetry (DPV). Using a conventional three-electrode system, a NiCo precursor/C was used as a working electrode; an Ag/AgCl electrode was used as a reference electrode, and a platinum electrode was used as a counter electrode.

3. Results and discussion

3.1. Characterization of NiCo Precursor/C

The morphology of the aligned carbon fibers with or without NiCo was measured using SEM. Figure 2(A) shows a carbon fiber before cobalt-nickel growth; the carbon fiber can be several centimeters long, and the degree of order can be controlled. Figures 2(B) and (C) are the microporous morphological NiCo complexes grown *in situ* on carbon fibers. Some studies have shown that nanomaterials and carbon fiber carriers constitute a core–shell structure, stabilizing the ultra-long structure and achieving more active shell properties [29–31]. Similar to figure 2(D), the microporous fossil structure, the NiCo alloy on the surface of the carbon fiber is arranged in the form of *Millepore sp.* on the surface of the carbon fiber (figure 2(B)). This morphology has high nanosheet density, meaning the ultra-long structure enlarges the specific surface area of the electrode, increases the charge flux, and further increases electron transport speed [32]. The patchwork of nanosheet alignments allows the carbon fiber surface to exhibit a porous structural feature that reduces the diffusion distance of the ions while allowing the electrolyte material to penetrate the interior of the active material [33, 34].

In order to understand its constituent components and structural characteristics, the precursor was subjected to crystal form analysis as well as elemental analysis. As seen in figure 3(A), the red, blue, and black

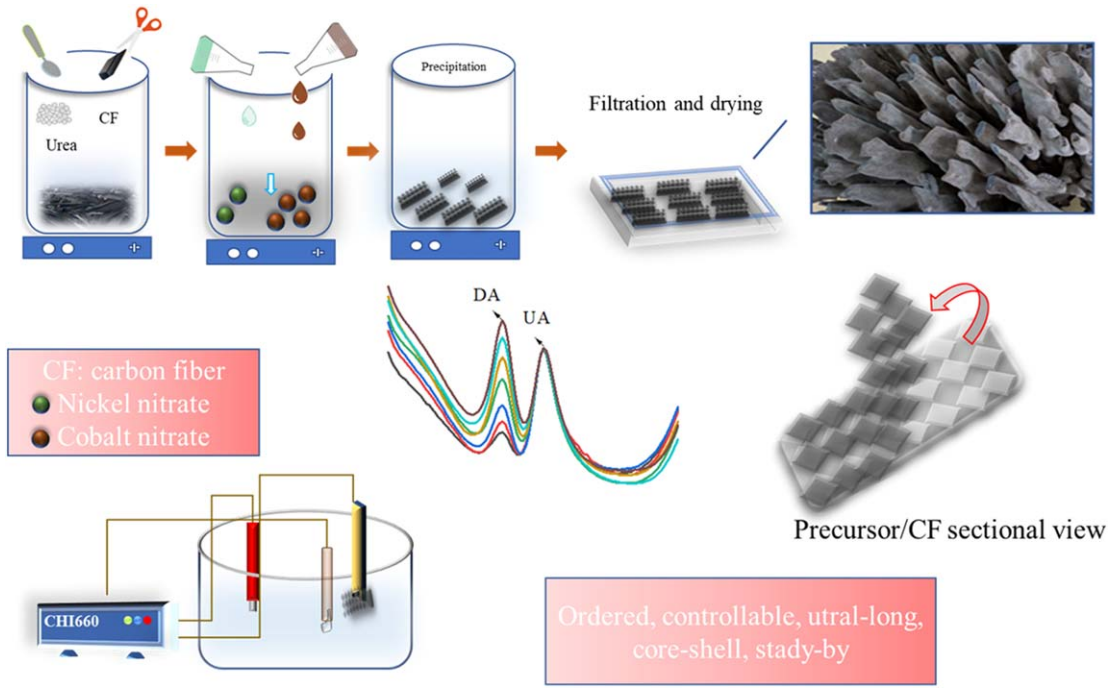

Figure 1. Preparation and electrochemical process of NiCo precursor/C.

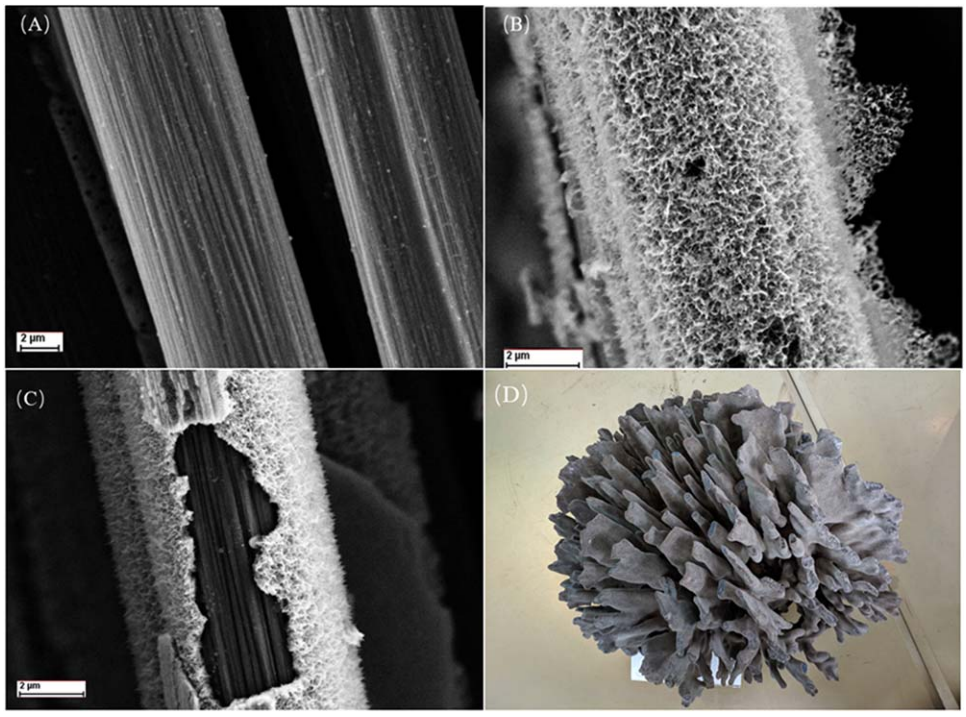

Figure 2. (A) SEM image of carbon fiber without the NiCo precursor, (B) and (C) high-power SEM image of the NiCo precursor/C, (D) morphology of *Millepore sp.* (Photographed at Nanjing Paleontology Museum).

curves represent XRD patterns of the NiO, Co_3O_4, and $NiCo_2O_4$ standards, respectively. Based on the intensity and width of the diffraction peak, we noticed that the addition of Ni decreased the crystallinity of the NiCo compound.

Figure 3(B) is the FT-IR of the precursor (400–4000 cm^{-1}); the broad peak of 3400 ccm^{-1} is the stretching vibration νOH of the adsorbed water on the material. The weak peak of 1600 cm^{-1} is the bending vibration δOH of water. The weak absorption peak at 2300 cm^{-1} is a typical vibration of the C≡N triple bond anion and

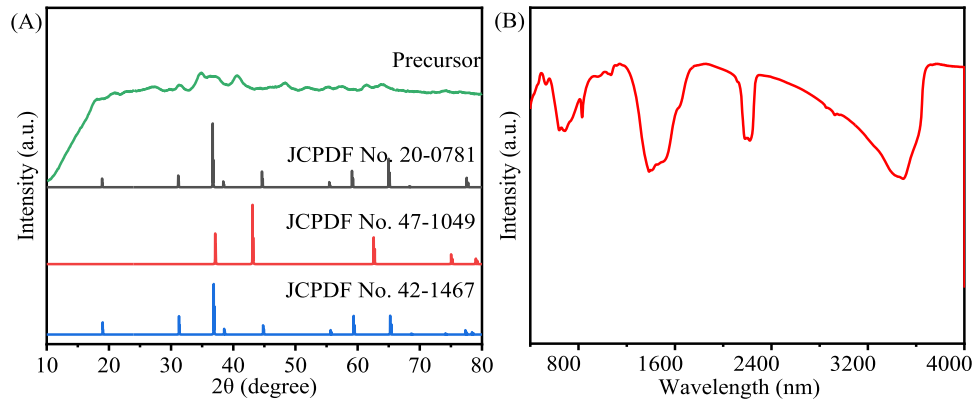

Figure 3. (A) XRD patterns, (B) FT-IR of the NiCo precursor/C.

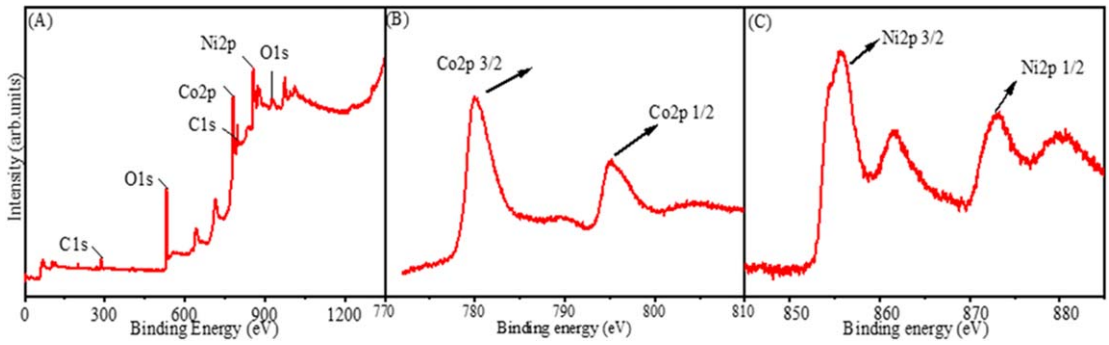

Figure 4. (A) XPS broad spectrum scanning of NiCo precursor/C and (B) high-resolution XPS of Co 2p, (C) Ni 2p.

represents a by-product of urea hydrolysis [35]. The 1300 cm^{-1} peak is attributed to CO_3^{2-} in the precursor. The peak below 1000 cm^{-1} is the vibration between the metal oxide atoms, which can be attributed to the oxidized composite of Ni and Co.

XPS provided surface information and characterized the oxidation state of the detection element. Figure 4 shows the spectra of the NiCo precursor and core grades Co 2p and Ni 2p. The Co 2p spectrum (figure 4(B)) is suitable for two spin–orbital double peaks at 780.3 eV Co $2p_{3/2}$ and 795.3 eV Co $2p_{1/2}$, representing the characteristics of Co^{2+} and Co^{3+}, and two not apparent vibration satellites [29]. The Ni 2p peak features two spin-orbital bimodal peaks at 855.8 eV Ni $2p_{3/2}$ and 873.2 eV Ni $2p_{1/2}$, representing Ni^{2+} and Ni^{3+}, while the spin-orbit bimodal is accompanied by two vibrating satellites located at 861.8 eV and 881.2 eV [36] (figure 4(C)). Based on the above composition analysis, we speculate that the composition of the precursor is $[MCO_3]x{\cdot}[M(OH)_2]y{\cdot}nH_2O$ (M = Co, Ni; x,y, n = 1–5).

3.2. Electrochemical characterization

The electrochemical properties of the NiCo precursor/C were investigated using a conventional three-electrode measurement with pH 7.0 PBS as the electrolyte on a CHI660E electrochemical workstation. The CV results for three substances (DA, UA) are shown in figure 5. Figure 5(A) is the CV of uric acid. From 0–0.8 V, only the oxidation peak of uric acid appeared at 0.35 V, indicating that UA irreversibly reacts to NiCo precursor/C. Figure 5(B) contains two oxidation peaks in the positive scan at −0.208 V, and one reduction peak during the negative scan at 0.151 V for dopamine. The additional irreversible dopamine oxidation peak during the positive scan corresponds to a dopamine oxidation intermediate (scheme 1); the presence or absence of intermediates is considered to be the key to demonstrating whether the electrochemical mechanism of DA is a single-electron transfer reaction or a two-electron transfer reaction [37, 38].

The CV of the NiCo precursor/C for two substances indicated that the two substances undergo different electrochemical processes. DPV has higher sensitivity than the CV and usually used for quantitative analysis of substances. Figure 6 show the DA and UA response of DPV at NiCo precursor/C working electrode when one concentration is kept constant, respectively. As shown in figures 6(A) and (C), the peak potentials of DA and UA are 0.19, and 0.34 V, respectively, and the two substances separate, a change in the content of one substance does

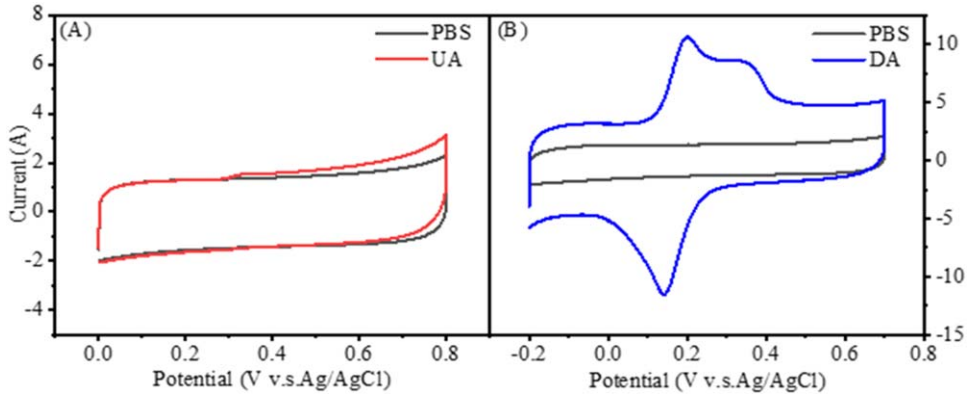

Figure 5. CV curves of (A)uric acid, and (B) dopamine in pH 7.0 PBS solution on the NiCo precursor/C composite electrode.

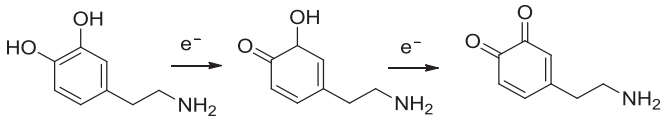

Scheme 1. Dopamine electrochemical process.

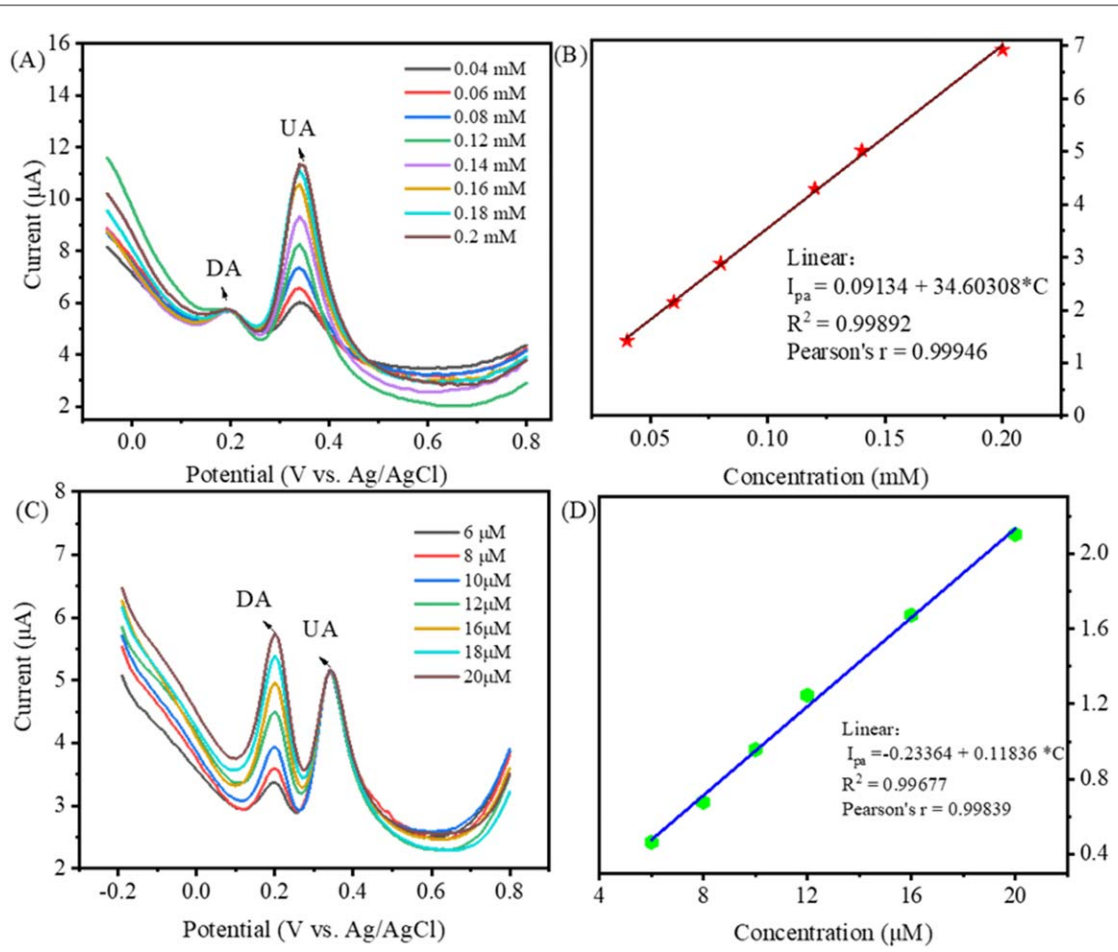

Figure 6. The DPV curve (A), (C) and the corresponding linear relationship (B), (D) when UA and DA exist in each other.

Table 1. UA and DA by DPV using different electrodes.

Electrode	Sensitivity (linear range). $\mu A\ \mu M^{-1}$ UA	DA	References
SnO_2	(10^{-1}–10)	—	[39]
GCE	0.66(1–200)	—	[40]
GCE	0.1	3.54 (0.1–20)	[41]
ZnO–CuxO/polypyrroe	0.2(0.5–70)	0.04(0.1–130)	[42]
Array of recessed Au /polymethylmethacrylate	6.38(20–170)	0.66(3.5–125)	[43]
ZnO/CF		9.84(5–70)	[44]
ZnO/CF	(20–200)		[45]
Pd /graphene/chitosan	(0.5–200)	(0.5–15) (20–200)	[46]
Graphene flowers /CF	(3.78–183.87)	(0.7–45.21)	[47]
nitrogen doped graphene	(0.1–20)	(0.5–170)	[48]
cobalt-nickel/CF	0.04–0.20 mM	6–20 μM	This work

not interfere with another substance. When UA has an increasing concentration from 0.04–0.20 mM with fixed 0.01 mM DA, the peak current of DA is stable and has a good linear. Plot concentration versus UA current, the linear relationship is $I_{pa1} = 34.60308\ C + 0.09134$ ($r = 0.9995$) seen in figure 6(B). That indicates that the presence of DA does not interfere with the detection of UA. Similarly, when UA in solution was present at 0.1 μM, DA was stable at 6–20 μM also had a good linear relationship. The linear relationship is $I_{pa2} = 0.11836\ C - 0.023364$ ($r = 0.9984$) seen in figure 6(D). The limit of detection for UA and DA are 0.027 mM and 0.175 μM, respectively, which acceptable performance compared with previous work (table 1).

Therefore, we have reason to conclude that there is negligible detection interference between DA and UA. Besides, this level of detection will overlap with the upper half of the clinically relevant range, with the upper part being associated with several diseases. NiCo precursor/C is expected to be used for the clinical application of DA and UA.

4. Conclusions

In this work, we used carbon fiber as a template to grow a NiCo material with a *Millepore sp.* morphology. The cobalt-nickel material shaped like *Millepore sp.* has a micro-nano hierarchical structure; the chemical formula is $[MCO_3]x{\cdot}[M(OH)_2]y{\cdot}nH_2O$ ($M = Co, Ni$; $x, y, n = 1$–5). Besides, the template used is controllable and ultra-long, no organics remains in the preparation process, and the NiCo precursor/C obtained can be directly used as an electrode. Electrochemical activity experiments showed that the composite shows good redox activity towards DA and UA with distinct, separate, individual electrochemical signals observed using DPV, the linear range for DA and UA is 6–20 μM and 0.04–0.20 mM, respectively, the detection limits are 0.175 μM and 0.027 mM, respectively, the standard deviation is 2.8% and 7.1%.

Acknowledgments

This work was supported by the National Natural Science Foundation of China (Grant Nos. 91644103, 41603104), the National Key Research and Development Program of China (2017YFC0212302), the Postdoctoral Foundation of Jiangsu Province (1601090B),the China Postdoctoral Science Foundation (2016M601694),and the Natural Science Foundation for Young Scientists of Jiangsu Province, China (BK20150895). Also including the Program for Changjiang Scholars and Innovative Research Team in University of Ministry of Education of China (PCSIRT) and the Priority Academic Program Development of Jiangsu Higher Education Institutions (PAPD). At the same time, we also thank Professor Yanlin Zhang for his support and discussion.

ORCID iDs

Chi Yang https://orcid.org/0000-0002-2569-9853

References

[1] Zhang N, Yu K, Li L and Zhu Z 2008 Investigation of electrical and ammonia sensing characteristics of Schottky barrier diode based on a single ultra-long ZnO nanorod *Appl. Surf. Sci.* **254** 5736–40

[2] Khandelwal V, Sahoo S K, Kumar A and Manik G 2017 Study on the effect of carbon nanotube on the properties of electrically conductive epoxy/polyaniline adhesives *J. Mater. Sci., Mater. Electron.* **28** 14240–51

[3] Gong F, Wang H, Xu X, Zhou G and Wang Z-S 2012 *In situ* growth of $Co_{0.85}Se$ and $Ni_{0.85}Se$ on conductive substrates as high-performance counter electrodes for dye-sensitized solar cells *JACS* **134** 10953–8

[4] Lee K, Shin S, Degen T, Lee W and Yoon Y S 2017 *In situ* analysis of SnO_2/Fe_2O_3/RGO to unravel the structural collapse mechanism and enhanced electrical conductivity for lithium-ion batteries *Nano Energy* **32** 397–407

[5] Fan H, Xu S, Cao X, Liu D, Yin Y, Hao H, Wei D and Shen Y 2017 Ultra-long Zn_2SnO_4-ZnO microwires based gas sensor for hydrogen detection *Appl. Surf. Sci.* **400** 440–5

[6] Yang S, Liu Y, Chen W, Jin W, Zhou J, Zhang H and Zakharova G 2016 High sensitivity and good selectivity of ultralong MoO_3 nanobelts for trimethylamine gas *Sensors Actuators* B **226** 478–85.

[7] Wang D, Hao C, Zheng W, Peng Q, Wang T, Liao Z, Yu D and Li Y 2008 Ultralong single-crystalline Ag_2S nanowires: promising candidates for photoswitches and room-temperature oxygen sensors *Adv. Mater.* **20** 2628–32.

[8] Li H, Liao J, Du Y, You T, Liao W and Wen L 2013 Magnetic-field-induced deposition to fabricate multifunctional nanostructured Co, Ni, and NiCo alloy films as catalysts, ferromagnetic and superhydrophobic materials *Chem. Commun.* **49** 1768–70

[9] Wu J, Ren Z, Du S, Kong L, Liu B, Xi W and Zhu H 2016 A highly active oxygen evolution electrocatalyst: Ultrathin CoNi double hydroxide/CoO nanosheets synthesized via interface-directed assembly *Nano Res.* **9** 713–25

[10] Yuan C, Li J, Hou L, Zhang X, Shen L and Lou X W 2012 Ultrathin mesoporous $NiCo_2O_4$ nanosheets supported on Ni foam as advanced electrodes for supercapacitors *Adv. Funct. Mater.* **22** 4592–7

[11] Yu L, Xia B Y, Wang X and Lou X W 2016 General formation of M–MoS_3 (M = Co, Ni) hollow structures with enhanced electrocatalytic activity for hydrogen evolution *Adv. Mater.* **28** 92–7

[12] Peng S *et al* 2014 MS_2 (M = Co and Ni) Hollow Spheres with tunable interiors for high-performance supercapacitors and photovoltaics *Adv. Funct. Mater.* **24** 2155–62.

[13] Wu H B, Pang H and Lou X W D 2013 Facile synthesis of mesoporous $Ni_{0.3}Co_{2.7}O_4$ hierarchical structures for high-performance supercapacitors *Energy & Environmental Science* **6** 3619–26

[14] Jia G, Hu Y, Qian Q, Yao Y, Zhang S, Li Z and Zou Z 2016 Formation of hierarchical structure composed of (Co/Ni) Mn-LDH nanosheets on MWCNT backbones for efficient electrocatalytic water oxidation *ACS Applied Materials & Interfaces* **8** 14527–34

[15] Liu Q, Xu X, Xia W, Che R, Chen C, Cao Q and He J 2015 Dependency of magnetic microwave absorption on surface architecture of $Co_{20}Ni_{80}$ hierarchical structures studied by electron holography *Nanoscale* **7** 1736–43

[16] Xu J, Wang Y, Yang C, Cao J, Chen Z and Ni C 2018 Design of high-performance core–shell hollow carbon nanofiber@nickel-cobalt double hydroxide composites for supercapacitive energy storage *J. Solid State Electrochem.* **22** 3853–62.

[17] Liu Y, Fu N, Zhang G, Xu M, Lu W, Zhou L and Huang H 2017 Design of hierarchical Ni□Co@ Ni Co layered double hydroxide core–shell structured nanotube array for high-performance flexible all-solid-state battery-type supercapacitors *Adv. Funct. Mater.* **27** 1605307

[18] Gao W, Huang H, Shi H, Feng X and Song W 2014 Nitrogen-rich graphene from small molecules as high performance anode material *Nanotechnology* **25** 415402

[19] Jaison J, Archana S, Saranyan V, Kumar T, Vijayamohanan K and Subbiah A 2018 Nickel-incorporated, nitrogen-doped graphene nanoribbons as efficient electrocatalysts for oxygen evolution reaction *J. Electrochem. Soc.* **165** H141–6

[20] Narayanan N T, Vineesh T V, Archana S, Sivamathini R and Alwarappan S 2017 Non-precious metal/metal oxides & nitrogen doped reduced graphene oxide based alkaline water electrolysis cell *Chem. Cat. Chem.* **9** 4295–300

[21] Vineesh T V, Mubarak S, Hahm M, Prabu V, Alwarappan S and Narayanan T 2016 Controllably alloyed, low density, free-standing Ni-Co and Ni-graphene sponges for electrocatalytic water splitting *Sci. Rep.* **6** 31202

[22] Wang X, Zheng Y, Yuan J, Shen J, Hu J, Wang A-J, Wu L and Niu L 2017 Three-dimensional NiCo layered double hydroxide nanosheets array on carbon cloth, facile preparation and its application in highly sensitive enzymeless glucose detection *Electrochim. Acta* **224** 628–35.

[23] Huo X, Liu X, Jin L, Sukumaran P and Wong D K Y 2016 Strategic applications of nanomaterials as sensing platforms and signal amplification markers at electrochemical immunosensors *Electroanalysis* **28** 1730–49

[24] Poksinski M, Dzuho H and Arwin H 2003 Copper corrosion monitoring with total internal reflection ellipsometry *J. Electrochem. Soc.* **150** B536

[25] Fu H J, Wang Y, Dong X, Liu Y, Chen Z J, Shen Y D, Yang C, Dong J and Xu Z 2016 Application of nickel cobalt oxide nanoflakes for electrochemical sensing of estriol in milk *RSC Adv.* **6** 65588–93.

[26] Powers D C and Ritter T 2012 Bimetallic redox synergy in oxidative palladium catalysis *Acc. Chem. Res.* **45** 840–50

[27] Joseph J *et al* 2014 Shape tailored $Ni_3(NO_3)_2(OH)_4$ nano-flakes simulating 3D bouquet-like structures for supercapacitors: exploring the effect of electrolytes on stability and performance *RSC Adv.* **4** 39378–85.

[28] Jiang X, Cheng W, Hu H, Hu Y, Cao Y and Yan S 2019 Facile preparation of a novel composite $CoNi(OH)_2$/carbon sphere for high-performance supercapacitors *Mater. Technol.* **34** 204–12.

[29] Zhao Y, Meng Y and Jiang P 2014 Carbon@MnO_2 core–shell nanospheres for flexible high-performance supercapacitor electrode materials *J. Power Sources* **259** 219–26.

[30] Wang D, Xin H L, Hovden R, Wang H, Yu Y, Muller D A, DiSalvo F and Abruña H 2012 Structurally ordered intermetallic platinum–cobalt core–shell nanoparticles with enhanced activity and stability as oxygen reduction electrocatalysts *Nat. Mater.* **12** 81

[31] Joo S H, Park J Y, Tsung C-K, Yamada Y, Yang P and Somorjai G A 2008 Thermally stable Pt/mesoporous silica core–shell nanocatalysts for high-temperature reactions *Nat. Mater.* **8** 126

[32] Lee H Y, Kim S W and Lee H Y 2001 Expansion of active site area and improvement of kinetic reversibility in electrochemical pseudocapacitor electrode *Electrochem. Solid-State Lett.* **4** A19–22

[33] Xu Z L, Huang J Q, Chong W G, Qin X, Wang X, Zhou L and Kim J 2017 *In situ* TEM study of volume expansion in porous carbon nanofiber/sulfur cathodes with exceptional high-rate performance *Adv. Energy Mater.* **7** 1602078

[34] Ma G, Guo D, Sun K, Peng H, Yang Q, Zhou X, Zhao X and Lei Z 2015 Cotton-based porous activated carbon with a large specific surface area as an electrode material for high-performance supercapacitors *RSC Adv.* **5** 64704–10

[35] Yan J, Fan Z, Sun W, Ning G, Wei T, Zhang Q, Zhang R, Zhi L and Wei F 2012 Advanced asymmetric supercapacitors based on $Ni(OH)_2$/graphene and porous graphene electrodes with high energy density *Adv. Funct. Mater.* **22** 2632–41.

[36] Chen J, Xu J, Zhou S, Zhao N and Wong C-P 2016 Amorphous nanostructured FeOOH and Co-Ni double hydroxides for high-performance aqueous asymmetric supercapacitors *Nano Energy* **21** 145–53.
[37] Simon P and Gogotsi Y 2008 Materials for electrochemical capacitors *Nat. Mater.* **7** 845–54.
[38] Corona-Avendaño S, Alarcón-Angeles G, Ramírez-Silva M T, Rosquete-Pina G, Romero-Romo M and Palomar-Pardavé M 2007 On the electrochemistry of dopamine in aqueous solution: I. The role of [SDS] on the voltammetric behavior of dopamine on a carbon paste electrode *J. Electroanal. Chem.* **609** 17–26
[39] Tatsuma T and Watanabe T Oxidase/peroxidase bilayer-modified electrodes as sensors for lactate, pyruvate, cholesterol and uric acid *Anal. Chim. Acta* **242** 85–9
[40] Guan Y, Wu T and Ye J 2005 Determination of uric acid and *p*-aminohippuric acid in human saliva and urine using capillary electrophoresis with electrochemical detection: potential application in fast diagnosis of renal disease *J. Chromatogr.* B **821** 229–34
[41] Dutt J S N, Cardosi M F, Livingstone C and Davis J 2005 Diagnostic implications of uric acid in electroanalytical measurements *Electroanalysis* **17** 1233–43
[42] Ghanbari K and Hajheidari N 2015 ZnO-CuxO/polypyrrole nanocomposite modified electrode for simultaneous determination of ascorbic acid, dopamine, and uric acid *Anal. Biochem.* **473** 53–62
[43] Zhang Y Q, Zhou Q, Zhao W, Chu W Y and Zheng J W 2016 Array of recessed gold nanoelectrodes formed with polymethylmethacrylate for individual detection of ascorbic acid, dopamine and uric acid *Electrochim. Acta* **212** 25–31
[44] Yang C, Gu B, Zhang D, Ge C and Tao H 2016 Coaxial carbon fiber/ZnO nanorods as electrodes for the electrochemical determination of dopamine *Analytical Methods* **8** 650–5
[45] Liu H, Gu C, Hou C, Yin Z, Fan K and Zhang M 2016 Plasma-assisted synthesis of carbon fibers/ZnO core–shell hybrids on carbon fiber templates for detection of ascorbic acid and uric acid *Sensors Actuators B* **224** 857–62
[46] Wang X, Wu M, Tang W, Zhu Y, Wang L, Wang Q, He P and Fang Y 2013 Simultaneous electrochemical determination of ascorbic acid, dopamine and uric acid using a palladium nanoparticle/graphene/chitosan modified electrode *J. Electroanal. Chem.* **695** 10–6
[47] Du J, Yue R, Ren F, Yao Z, Jiang F, Yang P and Du Y 2014 Novel graphene flowers modified carbon fibers for simultaneous determination of ascorbic acid, dopamine and uric acid *Biosens. Bioelectron.* **53** 220–4
[48] Sheng Z, Zheng X, Xu J, Bao W, Wang F and Xia X 2012 Electrochemical sensor based on nitrogen doped graphene: simultaneous determination of ascorbic acid, dopamine and uric acid *Biosens. Bioelectron.* **34** 125–31